Title
Attosecond transient-absorption dynamics of xenon core-excited states in a strong driving field

Journal
Physical Review A, 95(3)

ISSN
2469-9926

Authors
Kobayashi, Yuki
Timmers, Henry
Sabbar, Mazyar
et al.

Publication Date
2017-03-01

DOI
10.1103/physreva.95.031401

Peer reviewed

PHYSICAL REVIEW A **95**, 031401(R) (2017)

Attosecond transient-absorption dynamics of xenon core-excited states in a strong driving field

Yuki Kobayashi,[1] Henry Timmers,[1] Mazyar Sabbar,[1] Stephen R. Leone,[1,2,3,*] and Daniel M. Neumark[1,2,†]

[1]*Department of Chemistry, University of California, Berkeley, California 94720, USA*

[2]*Chemical Sciences Division, Lawrence Berkeley National Laboratory, Berkeley, California 94720, USA*

[3]*Department of Physics, University of California, Berkeley, California 94720, USA*

(Received 21 January 2017; published 9 March 2017)

We present attosecond transient-absorption experiments on xenon $4d^{-1}\,6p$ core-level states resonantly driven by intense (1.6×10^{14} W/cm^2) few-cycle near-infrared laser pulses. In this strongly driven regime, broad induced absorption features with half-cycle (1.3-fs) delay-dependent modulation are observed over the range of 58–65 eV, predicted as a signature of the breakdown of the rotating-wave approximation in strong-field driving of Autler-Townes splitting [A. N. Pfeiffer and S. R. Leone, Phys. Rev. A **85**, 053422 (2012)]. Relevant atomic states are identified by a numerical model involving three electronic states, and the mechanism behind the broad induced absorption is discussed in the Floquet formalism. These results demonstrate that a near-infrared field well into the tunneling regime can still control the optical properties of an atomic system over a several-electron-volt spectral range and with attosecond precision.

DOI: 10.1103/PhysRevA.95.031401

Coherent light-matter interactions modify the transparency of atoms and molecules [1]. Attosecond spectroscopy has paved the way for resolving temporal evolution of this laser-induced phenomenon, a topic related to the ultrafast control of optical properties of materials [2,3]. In a recent series of attosecond transient-absorption experiments, researchers have measured the subcycle absorption dynamics of rare gas atoms in resonant driving fields [4–10]. These experiments utilize attosecond extreme ultraviolet (XUV) pulses to launch the system into the Rydberg states and femtosecond near-infrared (NIR) pulses to induce couplings among electronic states.

The experiments so far have been performed in the relatively weak driving regime ($<1\times10^{13}$ W/cm^2) where one can observe the absorption peak shift triggered by one-photon coupling between different parity states (i.e., Autler-Townes splitting [11]) and half-cycle oscillations triggered by two-photon coupling between same parity states [6–10]. Theories suggest that in the strong driving limit where the rotating-wave approximation breaks down, half-cycle oscillations appear in addition to a large energy splitting even in the absence of the two-photon coupling [12]. However, here we experimentally demonstrate that this mechanism is possible in real atomic systems in the presence of other competing processes, such as strong-field ionization.

In this Rapid Communication, we perform attosecond transient-absorption spectroscopy on xenon $4d^{-1}\,6p$ states and experimentally investigate the absorption dynamics in the tunneling regime. The attosecond temporal resolution and the wide spectral coverage of our apparatus allow characterization of the entire absorption structure and the subcycle delay dependence in the strongly driven system; the latter feature was unresolved in a previous femtosecond experiment [13]. When driven at a field intensity of 1.6×10^{14} W/cm^2, the system shows both neutral and ionic state features. The neutral absorption peak originally at 65 eV is broadened down to 58 eV accompanied by half-cycle delay-dependent oscillations. Three-state model numerical simulations are performed, and the broad feature is identified as originating from the strong driving between $4d^{-1}\,6p$ and $4d^{-1}\,6s$ states. The mechanism behind the broad induced absorption and its subcycle delay dependence is intuitively explained within the Floquet formalism. Avoided crossings between Floquet states are found to play a significant role in the absorption dynamics of strongly driven systems.

A schematic of the experimental setup is shown in Fig. 1(a). Few-cycle carrier-envelope-phase stabilized NIR pulses (5 fs, 750 nm, 0.9 mJ, and 1 kHz) are generated by spectrally broadening the output of an amplified titanium sapphire laser system in a neon-filled stretched hollow core fiber. Isolated attosecond pulses are generated by directing part of the NIR beam through polarization assisted amplitude gating optics [14] and then performing high harmonic generation (HHG) in argon gas. The photon energy is centered at 67 eV [Fig. 1(b)], and the pulse duration is estimated to be 170 as by attosecond streaking from neon [15] [Fig. 1(c)]. The NIR and XUV beams are combined on an annular mirror, and then focused by a gold-coated toroidal mirror into an absorption gas cell of length 2 mm. Aluminum filters are placed after the HHG gas cell and the absorption gas cell to block the transmitted NIR pulse. Active-delay stabilization is implemented to achieve long-term stability of the interferometer by locking the phase of a spatial interference pattern from a 473-nm continuous laser beam [16]. Figure 1(d) shows the delay jitter recorded in the present measurement; the root-mean square of the jitter is measured to be <40 as. The transient spectra are recorded by the change in optical density (OD), $\Delta\mathrm{OD} = -\ln(I/I_{\mathrm{ref}})$, where I and I_{ref} represent the transmitted XUV intensity with and without the NIR pulse, respectively. At each delay step, the instantaneous ΔOD is averaged over 250 frames, and in each frame, I and I_{ref} are acquired for 100 laser pulses.

Figure 2(a) shows delay-dependent transient-absorption spectra at a field intensity of 1.6×10^{14} W/cm^2. The Keldysh parameter from the present conditions of ground-state xenon (ionization potential = 12.13 eV [17]) is $\gamma = 0.85$, indicating that the field intensity is in the tunneling regime [18]. Negative time delays correspond to the XUV pulses arriving prior to the

*srl@berkeley.edu

†dneumark@berkeley.edu

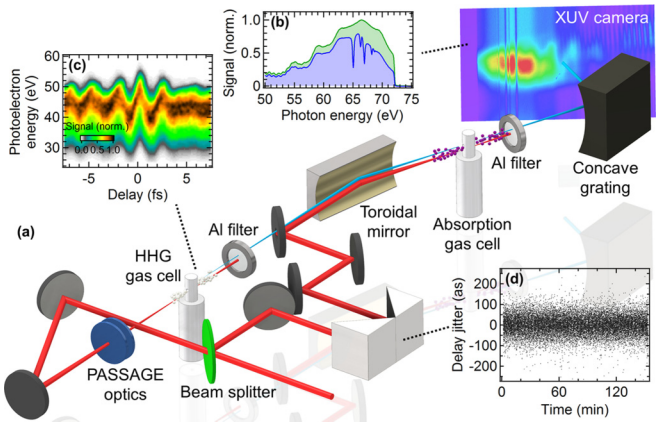

FIG. 1. (a) Schematic of the experimental setup. The red and blue beams represent NIR and XUV pulses, respectively. (b) XUV spectra with (blue shaded) and without (green shaded) xenon in the absorption gas cell. (c) An example of a streaking trace. The XUV pulse duration is retrieved to be 170 as. (d) Recorded delay jitter over the pump-probe measurement. The rms of the jitter is <40 as.

NIR pulses. Spectral assignments given on the right side of the panel are based on previous synchrotron-based charged-particle measurements [19,20]. At long negative delays (<-10 fs), one observes the effects of weak satellite pulses, primarily Autler-Townes splitting of the $4d^{-1}np$ series. The appearance of Autler-Townes splitting indicates the known resonant couplings in the $4d^{-1}np$ series induced by the NIR pulses. Ionic signals are seen at positive delays below 57 eV. Half-cycle buildup of the ion population is resolved, which is characteristic of strong-field ionization. The strong-field dynamics beyond the quasistatic picture can be characterized from this signal [21].

The most interesting feature in Fig. 2(a) is the broad induced absorption near zero delay, which spectrally extends from 58 to 65 eV. This broad bandwidth can only partially be understood from the inherent short lifetime of the autoionizing $4d_{5/2}^{-1}6p$ state ($\Gamma = 110$ meV, $\tau = 6$ fs) [19] and any additional lifetime shortening by strong-field ionization [9]. Variation of the pump-probe time delay yields half-cycle (1.3-fs) periodic modulation of the absorption signals over the entire spectral range. Averaged peak energies of the signals in the range of 62–65 eV are represented in Fig. 2(b) by the white line. The peak energies as well as the peak amplitudes are found to be modulated with half-cycle periodicity. As will be discussed later, this peak energy oscillation reflects the phase-dependent response of Floquet states in strong driving fields.

To identify the electronic states involved in the creation of the broad induced absorption, the absorption spectra are simulated by numerically solving the time-dependent Schrödinger equation for a three-state model. Atomic units are used throughout the following discussion.

The Hamiltonian of the three-state model takes the form

$$H(t) = \begin{pmatrix} 0 & d_{g1}E(t) & 0 \\ d_{g1}E(t) & \omega_1 - i\Gamma_1/2 & d_{01}E(t) \\ 0 & d_{01}E(t) & \omega_0 - i\Gamma_0/2 \end{pmatrix}, \quad (1)$$

where ω_i is energy of state i, d_{ij} are transition dipole moments, $E(t)$ is the electric field, and Γ_i is the lifetime of the

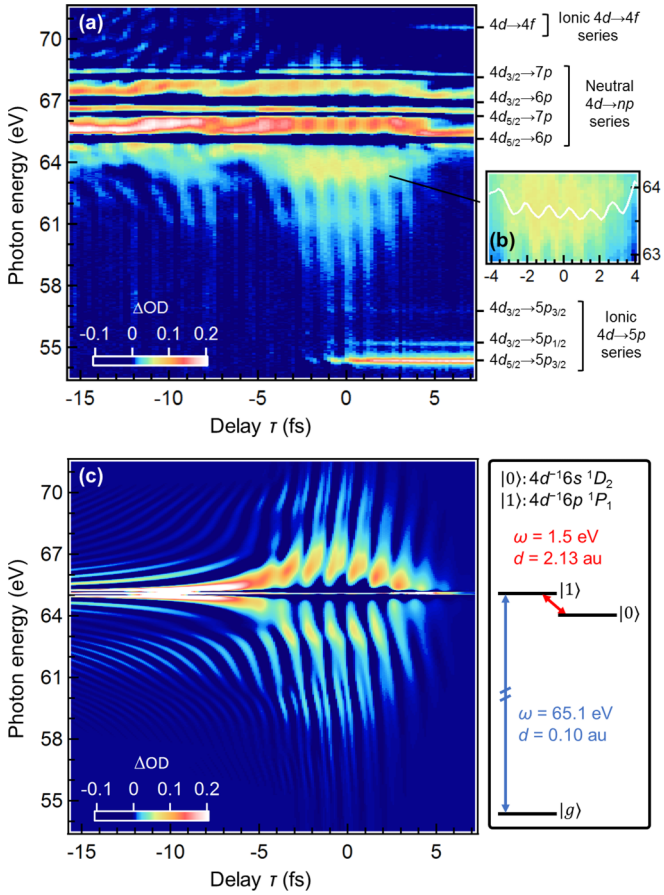

FIG. 2. (a) Experimental transient-absorption spectrum as a function of delay τ. The peak intensity of the NIR pulse is 1.6×10^{14} W/cm^2, and the delay step $\Delta\tau$ is 200 as. Assignments of the signals are given on the right side of the spectrum. (b) Averaged center of the peak from 62 to 65 eV overlaid on the absorption spectrum. (c) Transient-absorption spectrum simulated with the three-state model. The simulation does not include satellite NIR pulses that cause line-shape modulation at negative delays in the experimental results. The right panel shows energy levels, transition energies, and transition dipoles used in the simulation.

autoionizing state i. The electric fields of the NIR and the XUV pulses are defined as a product of a Gaussian envelope and a sinusoidal carrier wave. The energy levels and Γ_1 are taken from the literature [19,22], and Γ_0 is optimized in the simulation to match the experimental results. The transition dipoles are computed using the relativistic multiconfiguration Dirac-Hartree-Fock computation package GRASP2K [23]. The time evolution of the dipole moment $d(t)$ is Fourier transformed to compute the absorption cross section $\sigma(\omega) \propto \omega\,\mathrm{Im}[\tilde{d}(\omega)/\tilde{E}(\omega)]$ [24]. The experimental observable ΔOD is obtained assuming the Beer-Lambert law.

Figure 2(c) shows the simulated absorption spectra. The broad induced absorption is well reproduced in both the delay and the spectral domains. The hyperbolic sidebands around the main peak at large negative delays are the collapse of the Lorentzian absorption line shape due to the truncation of the dipole oscillation by the NIR pulse [25]. The simulation results lead to the conclusion that the $4d^{-1}6p(^1P_1)$ and the $4d^{-1}6s(^1D_2)$ states are responsible for the creation of the

broad induced absorption, and it is confirmed that the strong driving field can induce half-cycle oscillations even at a field well into the tunneling regime.

To gain physical insight into the broad absorption feature, we employ the Floquet theory and describe the evolution of the system in terms of Floquet states [24,26]. A two-level Hamiltonian driven by an external harmonic field is given as $H(t) = H_0 - A(t)\cos(\omega t + \varphi)$, where H_0 is a field-free Hamiltonian, A is the dipole coupling amplitude, and φ is a global phase. When A is constant in time, the Hamiltonian becomes periodic with a periodicity of $T = 2\pi/\omega$. In the case of a time-dependent $A(t)$, we can define instantaneous Floquet states for each instant in time [27]. According to the Floquet theorem, the periodicity guarantees the existence of the solutions that have the form $|\Psi(t)\rangle = |\phi_j(t)\rangle e^{-i\epsilon_j t}$, where ε_j are quasienergies and $|\phi_j(t)\rangle = |\phi_j(t+T)\rangle$ are Floquet states that have the same periodicity as the external field. It can be shown that Floquet states satisfy the eigenvalue equation that resembles the time-independent Schrödinger equation,

$$\mathcal{H}|\phi_j(t)\rangle = \epsilon_j|\phi_j(t)\rangle. \tag{2}$$

The modified Hamiltonian $\mathcal{H} = H - i\frac{d}{dt}$ is linear and Hermitian in an extended Hilbert space [28]. When $|\phi_j(t)\rangle$ is a solution of Eq. (2), then the following substitution:

$$\epsilon_j^{(n)} = \epsilon_j + n\omega, \quad \left|\phi_j^{(n)}(t)\right\rangle = |\phi_j(t)\rangle e^{in\omega t}, \tag{3}$$

also gives an equivalent solution with an integer n representing the associated photon number of each Floquet state. Note that the introduction of Floquet states $|\phi_j^{(n)}(t)\rangle$ in the extended Hilbert space is different from the Fourier expansion of Floquet states. As can be seen from Eq. (2), Floquet states and quasienergies are generalizations of stationary states and energies of time-independent Hamiltonians. Since $\mathcal{H}$ is Hermitian, Floquet states constitute an orthonormal basis set in the extended Hilbert space. In the present xenon model, generalized parity transformations $|0\rangle \to |0\rangle$, $|1\rangle \to -|1\rangle$, and $t \to t + T/2$ keep the Hamiltonian identical. Due to these symmetries, the Floquet states possess even and odd parities, such as the field-free states [29]. Dipole transitions from the ground state are allowed only for even-n states.

Approximate analytical expressions of quasienergies for two-level systems are known as $\epsilon_{0,1} = \frac{1}{2}\{-\omega \pm \sqrt{[\omega - \Delta J_0(\frac{2A}{\omega}) + \Delta^2 J_1^2(\frac{2A}{\omega})]}\}$, where Δ is the transition energy between the two field-free states and $J_i(x)$'s are Bessel functions of the first kind [30,31]. Figure 3(a) shows the quasienergies computed for the xenon model in resonant driving fields. The solid lines represent even-n states, whereas the dotted lines represent odd-n states. It can be seen that the external driving field creates an evenly spaced energy structure, and the interaction between the degenerate ($\Delta n = 0$) Floquet states causes energy splittings. In the weak-field limit, the energy splitting scales linearly with the driving field amplitude, and this behavior is equivalent to Autler-Townes splitting (orange arrows). When the driving field amplitude reaches $A \approx 2\Delta$, corresponding in the present xenon model to a field intensity of $I = 9\times10^{13}$ W/cm^2, the neighboring ($\Delta n = \pm 2$) Floquet states sharing the same parity exhibit avoided crossings (blue arrows).

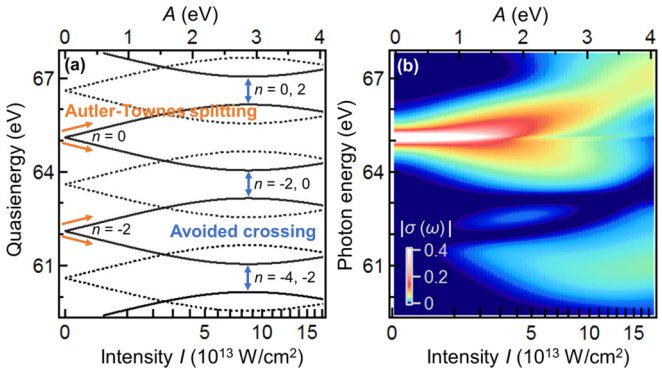

FIG. 3. (a) Quasienergy diagram of Floquet states as a function of driving field intensity. Solid and dotted lines represent even-n states and odd-n states, respectively. The atomic parameters are modeled for xenon. The bottom axis is plotted as a square root of the field intensity I, corresponding to a linear scale in the dipole coupling amplitude A. (b) Absorption cross section $|\sigma(\omega)|$ as a function of the driving field intensity simulated in the three-state model. The delay between the XUV and the NIR pulses is set to zero.

Figure 3(b) shows the absorption cross section $|\sigma(\omega)|$ as a function of the NIR field intensity simulated in the three-state model. Energy splittings are seen for both the main and the lower-lying signals, following the same lines as the quasienergy diagram as the field intensity increases. Around $I = 9\times10^{13}$ W/cm^2, the lower-lying absorption signals become more prominent. This behavior can be explained by the fact that the characteristics of the neighboring Floquet states are mixed across the avoided crossings and the $n = \pm 2$ Floquet states become brighter after the first avoided crossings. The quasienergy structure provides a straightforward interpretation of the absorption signals in strong driving fields. The spectral distribution of the broad induced absorption can be understood as being created by the large energy splitting beyond the avoided crossings.

We next consider the delay-dependent dynamics. Fourier transformation of the transient-absorption spectra in the delay-window $-5 < \tau < 5$ fs are shown in Figs. 4(a) and 4(b) for the experimental and the simulation results, respectively. In addition to the half-cycle dependence ($\omega = 3$ eV) over a broad range of photon energies, a weaker quarter-cycle dependence ($\omega = 6$ eV) is predicted at 61 eV in the simulated spectra.

Figures 4(c) and 4(d) show the delay dependence of the absorption signals at 63 eV simulated in the three-state model for two different global phases $\varphi = 0$ and $\varphi = \pi/2$, respectively. The vertical dotted lines are drawn to help compare the timing of the oscillations. We find that the variation of the phase caused in the delay-dependent oscillations at this photon energy is twice as large as the variation of the global phase. The effects of the global phase can clearly be factored out in the Floquet formalism [32,33]. Substituting the solution $|\Psi(t)\rangle = |\phi_j^{(n)}(t)\rangle e^{-i\epsilon_j^{(n)}t}$ into the time-dependent Schrödinger equation leads to

$$i\frac{\partial}{\partial t}\left|\phi_j^{(n)}(t)\right\rangle = \left(H_0 - \epsilon_j^{(n)}\right)\left|\phi_j^{(n)}(t)\right\rangle - \frac{A}{2}\left[\left|\phi_j^{(n+1)}(t)\right\rangle e^{i\varphi} + \left|\phi_j^{(n-1)}(t)\right\rangle e^{-i\varphi}\right]. \tag{4}$$

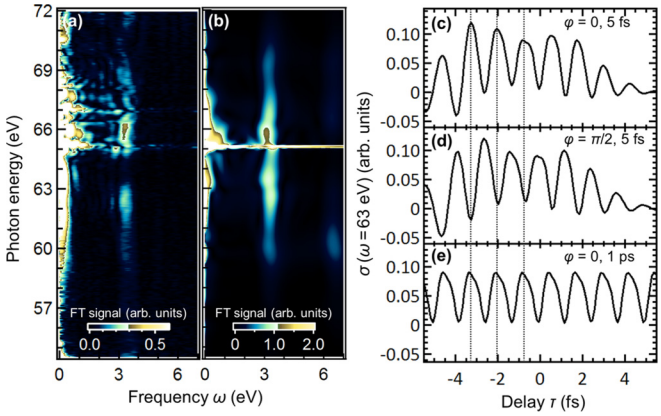

FIG. 4. (a) and (b) Fourier spectra along the delay interval $-5 < \tau < 5$ fs of the absorption measurements in the (a) experiments and (b) simulation. (c)–(e) Delay-dependent absorbance at 63-eV photon energy simulated in the three-state model for different pulse conditions: (c) $\varphi = 0$- and 5-fs pulses, (d) $\varphi = 0$- and 1-ps pulses, and (e) $\varphi = \pi/2$- and 5-fs pulses. Vertical lines are drawn to help compare the phase of the oscillations.

The φ dependence of the equation can be removed by introducing phase-shifted Floquet states,

$$\left|\tilde{\phi}_j^{(n)}\right\rangle = \left|\phi_j^{(n)}\right\rangle e^{in\varphi}. \tag{5}$$

This equation highlights the role of φ, namely, that it adds a phase shift of $n\varphi$ to the nth Floquet state.

The delay and the global phase can directly be connected by $\omega\tau = \varphi$ in a monochromatic wave case. However, since we use few-cycle broadband pulses in the experiments, the effects of the finite pulse duration need to be taken into account. The absorption signal simulated for a long-limit 1-ps driving pulse is shown in Fig. 4(e). No difference is seen regarding the half-cycle delay dependence compared with the 5-fs pulse results, and the variation of the pulse envelope is excluded from the mechanism of the delay dependence.

We may anticipate that the phase of the Floquet state is read out by the probing XUV pulse and imprinted onto the dipole moment. As exemplified by the Lorentz-to-Fano line-shape switching [34], varying the dipole phase modulates the absorption line shape. Indeed, the experimental results in Fig. 2(b) display periodic absorption line-shape modulation.

The current mechanism of the delay dependence is different from the interference between different transition pathways used previously to explain half-cycle oscillations [6]. The population of each Floquet state stays constant in the harmonic field except when nonadiabatic population transfer is triggered by the fast variation of the pulse envelope [27]. The comparison of the 5-fs and 1-ps pulse duration results in Figs. 4(c) and 4(e) verifies that nonadiabaticity does not contribute to producing the delay-dependent oscillation. The delay dependence rather represents the subcycle optical response of Floquet states to the probing fields. Although Floquet states have several analogous properties with conventional stationary states, their absorption signals do not necessarily give rise to a Lorentzian line shape. The absorption line shape changes depending on the relative timing between the driving pulse and the probing pulse.

The state mixing across the avoided crossings plays an important role in considering the photon number associated with each absorption line. The main absorption line around 65 eV, whose original photon number is $n = 0$, has both $n = 0$ and $n = \pm 2$ characters when the system is driven strongly beyond the avoided crossing. Since a pure $n = 0$ state exhibits no delay dependence, the half-cycle dependence is observed in the main absorption line only in a strong driving field [35]. This provides an alternative explanation to a phenomenon that has been regarded as the breakdown of the rotating-wave approximation.

To summarize, we have investigated attosecond absorption dynamics of light-dressed states created in the strongly driven xenon $4d^{-1}\,6p$ state. At a field intensity of 1.6×10^{14} W/cm^2, we have found significantly broadened absorption features and their half-cycle delay-dependent modulation. The numerical simulations reproduce the experimental findings and verify that subcycle optical control is possible for real atomic systems even in the tunneling regime. We have given physical interpretations within the Floquet formalism. It has been concluded that the state mixing across the avoided crossings is responsible for both the broad absorption structure and the subcycle delay dependence. Strong driving enables attosecond control of optical properties of materials over a broad range of the spectrum without being limited by the pulse duration. This methodology has general applicability to simple quantum systems and holds promise to be extended to condensed-phase matters for an application of ultrafast signal processing.

This material was based upon work supported by the U.S. Army Research Office (ARO) (Grant No. W911NF-14-1-0383) and the National Science Foundation (NSF) (Grant No. CHE-1361226). Y.K. acknowledges financial support from the Funai Overseas Scholarship.

[1] M. Fleischhauer, A. Imamoglu, and J. P. Marangos, Rev. Mod. Phys. **77**, 633 (2005).

[2] F. Krausz and M. Ivanov, Rev. Mod. Phys. **81**, 163 (2009).

[3] K. Ramasesha, S. R. Leone, and D. M. Neumark, Annu. Rev. Phys. Chem. **67**, 41 (2016).

[4] M. Chini, B. Zhao, H. Wang, Y. Cheng, S. X. Hu, and Z. Chang, Phys. Rev. Lett. **109**, 073601 (2012).

[5] S. Chen, M. J. Bell, A. R. Beck, H. Mashiko, M. Wu, A. N. Pfeiffer, M. B. Gaarde, D. M. Neumark, S. R. Leone, and K. J. Schafer, Phys. Rev. A **86**, 063408 (2012).

[6] M. Chini, X. Wang, Y. Cheng, Y. Wu, D. Zhao, D. A. Telnov, S.-I. Chu, and Z. Chang, Sci. Rep. **3**, 1105 (2013).

[7] X. Wang, M. Chini, Y. Cheng, Y. Wu, X.-M. Tong, and Z. Chang, Phys. Rev. A **87**, 063413 (2013).

[8] C. Ott, A. Kaldun, L. Argenti, P. Raith, K. Meyer, M. Laux, Y. Zhang, A. Blättermann, S. Hagstotz, T. Ding, R. Heck, J. Madroñero, F. Martín, and T. Pfeifer, Nature (London) **516**, 374 (2014).

[9] M. Reduzzi, J. Hummert, A. Dubrouil, F. Calegari, M. Nisoli, F. Frassetto, L. Poletto, S. Chen, M. Wu, M. B. Gaarde, K. Schafer, and G. Sansone, Phys. Rev. A **92**, 033408 (2015).

[10] W. Cao, E. R. Warrick, D. M. Neumark, and S. R. Leone, New J. Phys. **18**, 013041 (2016).
[11] S. H. Autler and C. H. Townes, Phys. Rev. **100**, 703 (1955).
[12] A. N. Pfeiffer and S. R. Leone, Phys. Rev. A **85**, 053422 (2012).
[13] M.-F. Lin, A. N. Pfeiffer, D. M. Neumark, S. R. Leone, and O. Gessner, J. Chem. Phys. **137**, 244305 (2012).
[14] H. Timmers, M. Sabbar, J. Hellwagner, Y. Kobayashi, D. M. Neumark, and S. R. Leone, Optica **3**, 707 (2016).
[15] E. Goulielmakis, V. S. Yakovlev, A. L. Cavalieri, M. Uiberacker, V. Pervak, A. Apolonski, R. Kienberger, U. Kleineberg, and F. Krausz, Science **317**, 769 (2007).
[16] M. Sabbar, S. Heuser, R. Boge, M. Lucchini, L. Gallmann, C. Cirelli, and U. Keller, Rev. Sci. Instrum. **85**, 103113 (2014).
[17] E. B. Saloman, J. Phys. Chem. Ref. Data **33**, 765 (2004).
[18] L. V. Keldysh, Sov. Phys. JETP **20**, 1307 (1965).
[19] O.-P. Sairanen, A. Kivimäki, E. Nõmmiste, H. Aksela, and S. Aksela, Phys. Rev. A **54**, 2834 (1996).
[20] P. Andersen, T. Andersen, F. Folkmann, V. K. Ivanov, H. Kjeldsen, and J. B. West, J. Phys. B **34**, 2009 (2001).
[21] M. Sabbar, H. Timmers, Y.-J. Chen, A. K. Pymer, Z.-H. Loh, S. G. Sayers, S. Pabst, R. Santra, and S. R. Leone, Nat. Phys., doi:10.1038/nphys4027 (2017).
[22] M. H. Miller, R. A. Roig, and R. D. Bengtson, Phys. Rev. A **8**, 480 (1973).
[23] P. Jönsson, X. He, C. F. Fischer, and I. Grant, Comput. Phys. Commun. **177**, 597 (2007).
[24] M. Wu, S. Chen, S. Camp, K. J. Schafer, and M. B. Gaarde, J. Phys. B **49**, 062003 (2016).
[25] M. Lindberg and S. W. Koch, Phys. Rev. B **38**, 7607 (1988).
[26] S.-I. Chu and D. A. Telnov, Phys. Rep. **390**, 1 (2004).
[27] K. Drese and M. Holthaus, Eur. Phys. J. D **5**, 119 (1999).
[28] H. Sambe, Phys. Rev. A **7**, 2203 (1973).
[29] A. Santana, J. M. G. Llorente, and V. Delgado, J. Phys. B **34**, 2371 (2001).
[30] C. Deng, J.-L. Orgiazzi, F. Shen, S. Ashhab, and A. Lupascu, Phys. Rev. Lett. **115**, 133601 (2015).
[31] C. Deng, F. Shen, S. Ashhab, and A. Lupascu, Phys. Rev. A **94**, 032323 (2016).
[32] V. Roudnev and B. D. Esry, Phys. Rev. Lett. **99**, 220406 (2007).
[33] J. J. Hua and B. D. Esry, J. Phys. B **42**, 085601 (2009).
[34] C. Ott, A. Kaldun, P. Raith, K. Meyer, M. Laux, J. Evers, C. H. Keitel, C. H. Greene, and T. Pfeifer, Science **340**, 716 (2013).
[35] M. Wu, S. Chen, M. B. Gaarde, and K. J. Schafer, Phys. Rev. A **88**, 043416 (2013).